Simulating Confined Explosions using Eulerian Multi-material Method

Jack J. Yoh[1], **Ki-hong Kim**[1]

[1]Department of Mechanical and Aerospace Engineering,
Seoul National University,
Seoul, Korea, 151-744

1 Multi-material explosive shock physics

High-speed impact of materials generates strong shock waves, large rates of deformations and generates hydrodynamic pressures that are often much greater than the deviatoric stresses. Then, variants of the standard Euler equations for compressible flow can be used to model materials with deviatoric strength. The dominant physical mechanisms satisfy the Euler equations to a first approximation, and the effects associated with deviatoric strength are in some sense a small correction. We describe the numerical methodology that we used to construct a high resolution (in both space and time) code that can be used to simulate multi-material interactions at high strain rates and explosive dynamics.

A set of comprehensive thermo-mechanical-chemical models are built for both energetic and metal elements of materials under study. The endothermic decomposition of explosives followed by rapid exothermic reactions possibly leading to a detonation is modeled with the latest global chemical kinetics reported in the literature [1, 2, 3]. The material models include gamma law for inert gas while the JWL equation of state (EOS) is used for the condensed phase hot product gas. The 7-term polynomial EOS is used for the unreacted solid explosive, and Mie–Gruneisen EOS for metals and other inerts. The failure of containment due to explosive dynamics is modeled by the modified Johnson-Cook failure model.

The present shock-physics multi-material code is suitable for simulating high-speed impact and interaction of energetic and inert materials. Energetic materials are modeled by the reactive Euler equations. The inert materials can be modeled by either the Euler equations or by constitutive laws that can describe metals. An extended level set based ghost-fluid approach is developed that can elegantly handle multi-material interfaces between virtually 'any' type of materials with large density gradients. A new technique is used to extrapolate material states into extended ghost nodes to enforce natural boundary conditions. The algorithms are verified with a collection of standard test problems that include: ZND wave, Taylor impact, and shock induced void(bubble) collapse in solid and fluid.

2 Chemical models of HMX, aluminized RDX, and TATB

The four-step, five-species reaction mechanism for HMX is

$$\mathrm{A} \rightarrow \mathrm{B}, \qquad r_1 = Z_1 \exp(-E_1/RT)\,\rho_{\mathrm{A}} \tag{1}$$

$$\mathrm{B} \rightarrow \mathrm{C}, \qquad r_2 = Z_2 \exp(-E_2/RT)\,\rho_{\mathrm{B}} \tag{2}$$

$$\mathrm{C} \rightarrow \mathrm{D}, \qquad r_3 = Z_3 \exp(-E_3/RT)\,\rho_{\mathrm{C}} \tag{3}$$

$$\mathrm{D} \rightarrow \mathrm{E}, \qquad r_4 = Z_4 \exp(-E_4/RT)\,\rho_{\mathrm{D}}^2 \tag{4}$$

where A and B are solid species (β- and δ-phase HMX), C is a solid intermediate, D and E are intermediate and final product gases, respectively[3, 1]. The reaction sequence is (i) β-HMX to δ-HMX, (ii) δ-HMX to solid intermediates, (iii) solid intermediates to gaseous intermediates (CH_2O, N_2O, HCN, HNO_2, etc.), and (iv) gaseous intermediates to final products (CO_2, H_2O, N_2, CO, C, etc.). Here r_i is the mass reaction rate, Z_i is the frequency factor, and E_i is the activation energy for reaction i. Also ρ_j is the mass concentration for species $j = A, B, C, D, E$.

The three-step, four-species reaction mechanism for RDX is

$$\mathrm{A} \rightarrow \mathrm{B}, \qquad r_1 = Z_1 \exp(-E_1/RT)\, \rho_\mathrm{A} \tag{5}$$

$$\mathrm{B} \rightarrow \mathrm{C}, \qquad r_2 = Z_2 \exp(-E_2/RT)\, \rho_\mathrm{B} \tag{6}$$

$$\mathrm{C} \rightarrow \mathrm{D}, \qquad r_3 = Z_3 \exp(-E_3/RT)\, \rho_\mathrm{C}^2 \tag{7}$$

where A and B are solid species, and C and D are product gases[2]. The mechanism for aluminized RDX requires a modification to the above steps; the second exothermic reaction step is replaced by the following,

$$\mathrm{B} \rightarrow \mathrm{C} + Al, \qquad r_2 = Z_2 \exp(-E_2/RT)\, \rho_\mathrm{B} \tag{8}$$

where Al, a constituent of species B, is treated as both inert and reactive until completion.

The third explosive for chemical kinetics consideration is TATB. The chemical decomposition kinetics are known with the following 3-step, 4-species reaction mechanism[1].

$$\mathrm{A} \rightarrow \mathrm{B} + H_2O, \qquad r_1 = Z_1 \exp(-E_1/RT)\, \rho_\mathrm{A} \tag{9}$$

$$\mathrm{B} \rightarrow \mathrm{C}, \qquad r_2 = Z_2 \exp(-E_2/RT)\, \rho_\mathrm{B} \tag{10}$$

$$\mathrm{C} \rightarrow \mathrm{D}, \qquad r_3 = Z_3 \exp(-E_3/RT)\, \rho_\mathrm{C}^2 \tag{11}$$

The decomposing solid TATB, A, produces intermediate solid B with water. The intermediate B is further decomposed into another solid intermediate C. The final exothermic reaction shown in step three is where the final product gas D is produced. For both solid reactions in steps one and two, the order of reaction is first while the gas production step in three is second order.

After the chemical reactions have progressed significantly into the explosive (burning) stage where approximately 20% of the energetic material is converted to product gases, the finite chemistry is no longer solved explicitly. Instead, a burn front model is used in which reactants are converted completely to products in a single reaction step. The burn rate velocity, V is assumed to be a pressure-dependent function, $V = aP^n$, where V is in mm/s and P is in MPa.

In addition to these explosives, hte model also considers several other gas mixtures such as acetylene-air and ethylene-air[4].

3 Calculations

Several calculations for validation include multi-material contact problems involving solids, gas, and liquid exposed to external stimuli.

3.1 ZND structure

Figure 1 shows the code is capable of maintaining a stable 1-D ZND detonation wave structure. The spatial structure perfectly overlays that obtained by integrating the steady ODEs for the ZND structure. The end states of the CJ detonation are found in [5]. The computed reaction zone thickness is 4 mm, and the steady CJ detonation propagates at a speed 8.0×10^3 m/s.

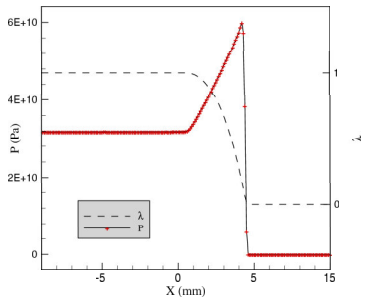

Figure 1: ZND detonation structure calculated by the current reactive solver. Δx is 0.1 mm, and consequently 40 points are placed in the 4 mm reaction zone.

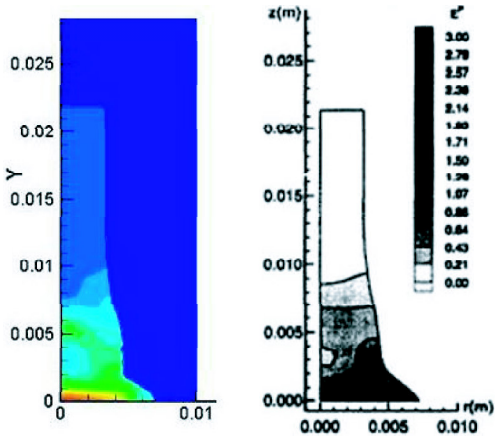

Figure 2: Grid comparison: (a) Calculated effective plastic strain field at time $t = 80\,\mu$sec by present method; (b) FEM calculation by Camacho & Ortiz (1997)

3.2 Taylor anvil test

A cylindrical copper rod of initial radius of 3.2 mm and a length of 32.4 mm strikes a rigid wall head-on at a velocity of 227 m/s. Figure 2 shows the calculated deformation at time $t = 80\,\mu$sec compared to a benchmark FEM calculation. The computed plastic strain field is in excellent agreement with a maximum value of 3.

3.3 Shock induced bubble (void) collapse

The third exercise includes high speed deformation of helium bubble in 2-D shock tube. Test set-up is analogous to a standard void collapse experiment often conducted in characterizing high explosives subject to mechanical insults. Shown in figure [?] is the before and after shots of shock deformation of a bubble. The ghost boundaries handle the deforming bubble interface.

In the final paper, we will report on the modeled bubble ingition and hot-spot ignition in energetic solids. Metal additives such as alumimum and magnesium which are known to enhance exothermic

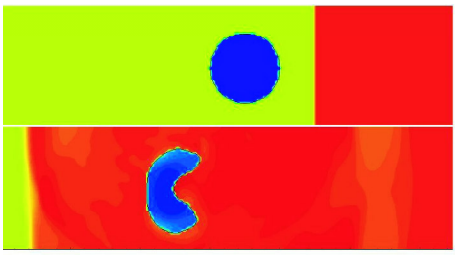

Figure 3: Shock induced bubble (void) collapse

reaction are added to the reactive flow.

4 Discussions

We have developed a comprehensive numerical framework to compute multi-material interactions for energetic and inert materials such as metals. The high-resolution simulation tool is carefully validated through a series of one-dimensional and multi-dimensional tests for simulating general confined explosions invovling explosives and gaseous fuels.

5 Acknowledgments

The authors are grateful to a list of funding agencies through which the projects HEMRC-HM-21, HEMRC-HM-22, and KRF-2005-003-D00057 were conducted. The additional support from the Brain Korea 21 through the Institute of Advanced Aerospace Technology at the Seoul National University is also acknowledged.

References

[1] Tarver, C. M., Chemical Kinetic Modeling of HMX and TATB Laser Ignition Tests. *Journal of Energetic Materials*, **22**, pp. 93–107, 2004.

[2] Yoh, J. J., McClelland, M. A., Maienschein, J. L., Wardell, J. F., and Tarver, C. M., Simulating Thermal Explosion of RDX-based Explosives: Model Comparison with Experiment. *Journal of Applied Physics*, **97**, 083504, 2005.

[3] Yoh, J. J., McClelland, M. A., Maienschein, J. L., Nichols, A. L., and Tarver, C. M., Simulating Thermal Explosion of HMX-based Explosives: Model Comparison with Experiment. *Journal of Applied Physics*, **100**, 073515, 2006.

[4] Oran, E. S., Gamezo, V. N. (2006), Origins of the deflagration-to-detonation transition in gas-phase combustion. Combustion and Flame, in press.

[5] Yoh, J. J., Stewart, D. S., High-Resolution Numerical Modeling of Energetic and Inert Materials at Large Deformation Rates. (2002), Lawrence Livermore National Laboratory, UCRL-JC-151176.